ON-CHIP CHARACTERIZATION OF STRESS EFFECTS ON GYROSCOPE ZERO RATE OUTPUT AND SCALE FACTOR

Erdinc Tatar[1], Tamal Mukherjee[1], and Gary K. Fedder[1, 2]
[1]Department of Electrical and Computer Engineering
[2]The Robotics Institute, Carnegie Mellon University, Pittsburgh, USA

ABSTRACT

Stress effects on performance are quantified for a vacuum packaged silicon-on-insulator (SOI) MEMS gyroscope, including zero rate output (ZRO), scale factor (SF), and resonance frequencies. On-chip environmental sensors comprising released SOI-silicon resistors in a bridge measure the temperature and stress separately. Experimental results from a four-point bending test-bed lead to a system model to compensate the gyroscope ZRO using the environmental sensor outputs. The ZRO shift varied linearly with stress, with a measured maximum of 3.5 °/s for 533 kPa applied external stress.

INTRODUCTION

Achieving long term MEMS gyroscope stability and sub-degree per hour bias instability requires compensation of the gyroscope output with environmental changes such as temperature [1]. Slowly varying environmental conditions (e.g., temperature and stress) limit the gyroscope stability over long run times. Gyroscope bias compensation with temperature [1, 2], and quadrature signal [2] have been reported to improve the long term MEMS gyroscope stability. Measuring the temperature on-chip provides a better assessment of the actual gyroscope temperature compared to off-chip measurements [2]. However as the temperature changes, inevitable thermal coefficient of expansion (TCE) mismatches between the MEMS die and surroundings exert stress as large as 50MPa on the die through the device spring anchors [3]. The common approach for gyroscope compensation considers temperature as the only environmental variable [1-2]. This work focuses on characterizing the gyroscope bias by measuring the on-chip stress and temperature separately. Knowing the stress and temperature independently may lead to a more effective bias compensation.

Our previous works have demonstrated temperature driven stress effects on gyroscope resonance frequencies [4], and pure stress effects on gyroscope resonance frequencies with three- and four-point bending test-beds [5]. References [4] and [5] demonstrate that MPa level stress affects the gyroscope resonance frequencies at levels comparable to temperature effects. Gyroscope resonance frequencies shift as a result of anchor displacements changing the spring constant.

A system level simulation technique was developed relating stress to ZRO and SF in a circuit simulation environment [6]. Stress leads to drive and sense comb mismatches through non-equal anchor displacements of the stator and rotor that generate a ZRO signal indistinguishable from the Coriolis signal. This work uses a four-point bending test-bed similar to [5] but adds on-chip stress and temperature sensors to the SOI-MEMS gyroscope and experimentally validates the simulation trends in [6]. The gyroscope is vacuum packaged by using an in-house developed system and tested in the closed loop drive and open-loop sense configuration.

ON-CHIP STRESS SENSORS

Figure 1.a shows the SEM image of the three-fold-symmetric SOI-MEMS gyroscope along with the location of the stress sensors highlighted. The electrostatic combs are symmetric so either of the two modes can be used as drive or sense with the frequency tuning capability. The stress sensors are located at the four sides of the gyroscope. Each stress sensor comprises four released SOI-silicon resistors connected in a Wheatstone bridge configuration to cancel out the temperature variations as shown in Figure 1.d. Since the SOI device layer is highly doped, the resistors are meandered to have a high resistance in the constrained space. Figure 1.b presents the stress and temperature sensitive silicon resistors that are series connected fixed-fixed beams. The stress insensitive, temperature sensitive resistors are released folded silicon beams as in Figure 1.c. Alignment of the anchors determines the stress sensitivity. Each SOI-silicon resistor value is $1.7\ k\Omega \pm 2\%$. The stress measurements were performed by applying a 5 V DC voltage across the bridge and reading the bridge output with a multimeter. Stress sensors at each side measure their respective axial component of the in-plane stress.

Figure 2 shows the oven test results of the resistance change vs. temperature for the stress sensitive and insensitive resistors. They both exhibit a positive temperature coefficient of resistance (TCR) of +0.0016 verifying the ability to cancel temperature with the bridge. Figure 3 shows the resistance changes for the stress sensitive and insensitive resistors when stress is applied to the die. The stress insensitive resistors do not exhibit any change proving their operation as pure temperature sensors.

Vacuum packaging of the gyroscope is critical in terms of testing and suppressing the Brownian noise. The gyroscope in this study is in-house vacuum packaged by using 40 pin off-the-shelf ceramic dual inline packages (DIP) and metal lids. Low temperature indium solder preforms are used to bond the lid and DIP. A titanium based getter, similar to [7], is deposited on the metal lid for long term stable vacuum. The vacuum packaged gyroscopes have quality factors (Q) varying between 4500 and 8000, and the variation is believed to be a result of the outgassing period before the packaging. Vacuum packaging has been successfully repeated on 5 gyroscope dies. The estimated pressure is in the rage of 150-300 mTorr with no leaks detected for more than one month.

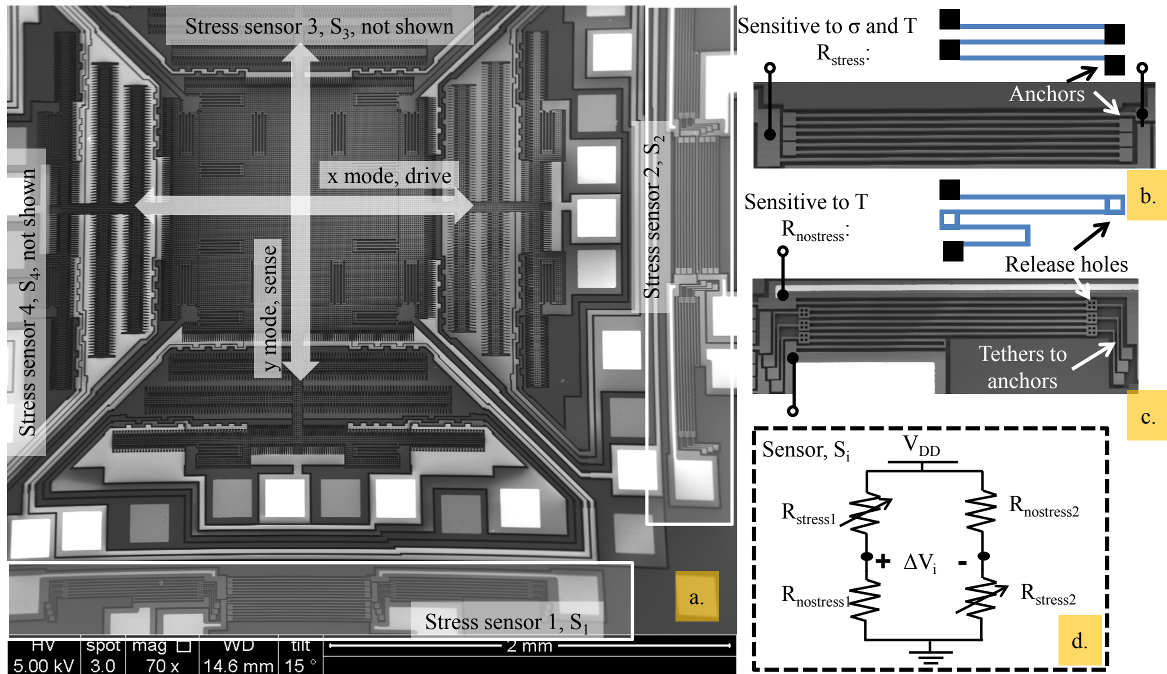

Figure 1: (a) Three-fold symmetric SOI-MEMS gyroscope highlighting the location of the stress sensor elements. (b) Stress and temperature sensitive fixed-fixed SOI-silicon beam resistor. (c) Stress-insensitive folded SOI-silicon beam resistor. (d) Wheatstone bridge.

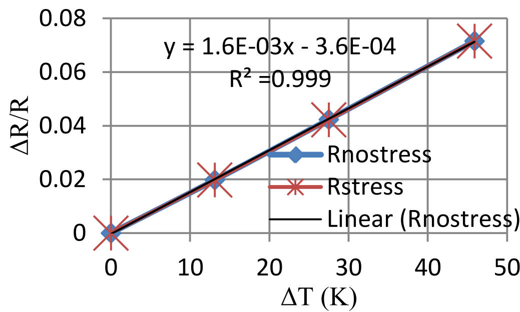

Figure 2: Resistance change vs. temperature test results in oven test, both resistors react similarly to the temperature verifying the Wheatstone bridge operation.

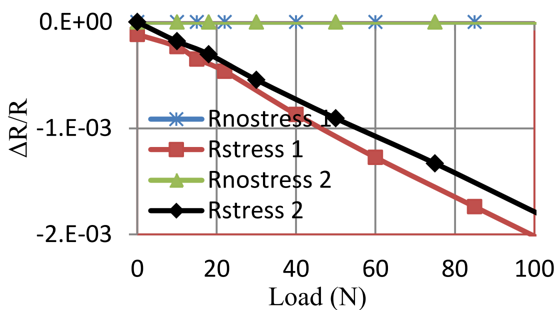

Figure 3: Resistance change with the stress applied to the die. Stress insensitive resistors do not react.

EXPERIMENTAL RESULTS

Although the two modes were identically designed in the layout, systematic frequency mismatches of 150-200 Hz have been observed in our previous designs [4]. Two possible reasons for the mismatch are a 30 nm raster-scanned mask linewidth mismatch or the 5° misaligned <111> silicon device layer. We have learned that although not specified, most commercial p-type <111> silicon wafers are cut 5° off axis. The frequency mismatch has been decreased by intentionally offsetting the beam width of springs of the corresponding mode as part of the design. The resonance frequencies for the gyroscope generating the results below are 8.6 kHz with 4 Hz mismatch without frequency tuning. Frequency mismatches as low as 2 Hz have been observed on the other dies.

The gyroscope is tested at a tuned 18 Hz mismatch under zero stress with $f_{drive} < f_{sense}$. A Zurich Instruments HF2LI lock-in amplifier was used to control the gyroscope. Transimpedance amplifiers on the PCB convert the gyroscope output current to voltage and the voltage outputs are fed to the lock-in amplifier for demodulation and control loops. The gyroscope is operated at closed loop drive with a PLL locking on the resonance frequency and amplitude stabilization loop and open loop sense mode.

Figure 4 shows the four-point bending stress test-bed used during the experiments along with the photograph of the vacuum packaged gyroscope. The gyroscope PCB is sandwiched in-between the steel cylinders that are held by the aluminum fixtures. Adding weights on top of the setup creates compressive bending stress on the gyro changing its characteristics. The goal of this test is finding the coefficients between the gyroscope ZRO and stress sensor outputs.

The weights ("load" in Figure 4) on the gyroscope are incremented with 5 lbs steps up to 15 lbs during the tests. At each step, gyroscope ZRO, stress on both axes and temperature (with a temperature sensing resistor) are recorded for 6 minutes, followed by a SF test on the rate table at ±5°/s and ±10°/s to compute the rate referred ZRO. Stress sensors 1 and 2 (S_1 and S_2 in Figure 1) are used capture the strain in the sense and drive axes, respectively. The stress test-bed was set up on the rate

table for continuous testing. The primary drift source in the experiments is believed to be the external stress since the measured on-chip temperature variation was less than 0.02°C.

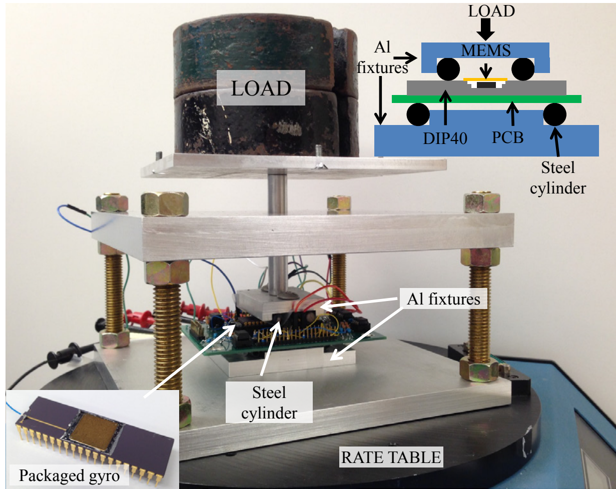

Figure 4: Four-point bending stress test-bed used to test the vacuum packaged gyroscope on the rate table. Adding weights on the gyroscope creates compressive bending stress.

Figure 5 shows the orientation of the die and transformation matrix that relates the measured stress and gyroscope parameters at constant temperature. This matrix is a step towards full model-based stress compensation. Each performance parameter has a dominant stress coefficient and a minor stress coefficient that is at least five times less sensitive. The dominant stress term for each gyroscope parameter is highlighted. The gyroscope is mounted 45° with respect to the package to result in nominally equal package-induced stress on both modes for better initial resonant frequency matching.

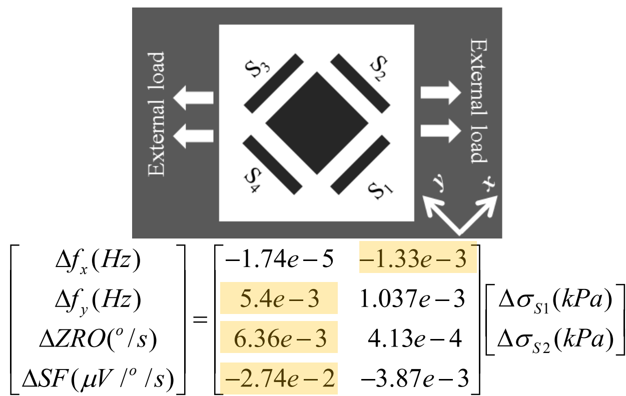

$$\begin{bmatrix} \Delta f_x(Hz) \\ \Delta f_y(Hz) \\ \Delta ZRO(^o/s) \\ \Delta SF(\mu V/^o/s) \end{bmatrix} = \begin{bmatrix} -1.74e-5 & -1.33e-3 \\ 5.4e-3 & 1.037e-3 \\ 6.36e-3 & 4.13e-4 \\ -2.74e-2 & -3.87e-3 \end{bmatrix} \begin{bmatrix} \Delta\sigma_{S1}(kPa) \\ \Delta\sigma_{S2}(kPa) \end{bmatrix}$$

Figure 5: Orientation of the die and the transformation matrix between stress and gyroscope parameters, each term is dominated by a single stress component.

Figures 6 and 7 show the resonance frequency vs. dominant stress for drive and sense modes, respectively. The stress sensor outputs provide an approximately linear estimation of the resonance frequency shifts from the baseline. The stress is negative since the four-point bending test exerts compressive stress on the die. Drive and sense frequencies primarily shift with stress along their respective orthogonal axis since their flexural spring constant is primarily affected by longitudinal stress [4]. Both mode frequencies have a repeatable relationship with compressive stress; however the sign of drive frequency response is counterintuitive. A decrease in the resonance frequency is expected with compressive stress. Although the 45° mounting equalizes the stress, we believe the drive mode is pre-stressed due to the possible deviations from the 45° angle and variation in the die bonding. The relatively low stress (< 1MPa) applied during the tests is not sufficient for the drive frequency to start decreasing.

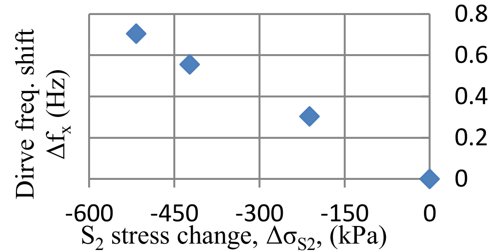

Figure 6: Linear drive mode resonance frequency shift vs. drive axis stress(S_2).

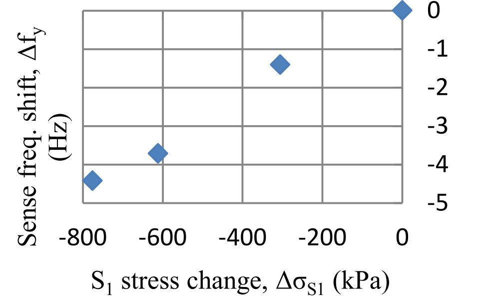

Figure 7: Linear sense mode resonance frequency shift vs. sense axis stress (S_1).

Figure 8 presents the SF test results as a function of the dominant sense mode stress (S_1) showing the increase with increasing stress. Since $f_{drive} < f_{sense}$ and the sense resonance frequency decrease is larger than drive frequency increase, reduced mismatch leads to increasing SF in open-loop operation. SF relates mainly to S_1 because the sense frequency shift is considerably larger than the drive frequency shift.

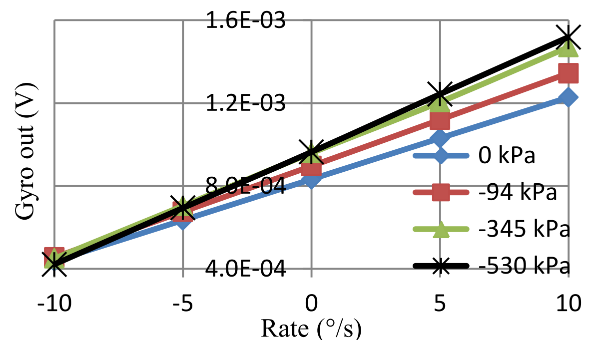

Figure 8: Scale factor test results for different stress levels on sense mode stress sensor (S_1).

Figure 9 shows the rate-referred ZRO change vs. the sense axis stress. The ZRO shift is believed to be originating from drive and sense comb gap mismatches. A drive comb gap mismatch generates a Coriolis in-phase

force on the sense mode, and leaks to the rate output because of the finite drive axis spring constant of the sense axis springs [6]. A sense comb mismatch on the other hand, increases the SF since an imbalance in the combs results in higher capacitive sensitivity. As the sense axis stress is larger than the drive axis stress in the tested gyroscope, sense comb mismatches increase the SF faster than ZRO which is dominated by the drive comb mismatches leading to a decrease in rate referred ZRO. Although the impressed stress is small (< 1MPa), Figure 9 shows that external stress at 100 kPa levels leads to °/s bias shifts.

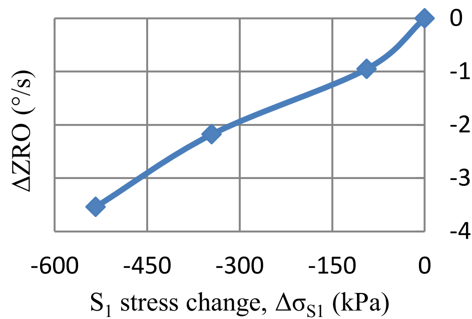

Figure 9: Zero rate output vs. sense axis stress.

After the matrix coefficients are obtained the logical next step is to explore output compensation. However, the stress sensors on the tested die failed due to electrostatic pull down to the substrate and subsequent short circuit. The 600 µm-long 5 µm wide 15 µm-thick stress sensor beams are suspended over the 2 µm SOI gap. Therefore, special attention must be paid to prevent electrostatic pull-down from the high DC potential (V_{PM}, 20V-40V DC) on the SOI substrate that is biased at the same potential as the proof mass. The problem is solved by biasing one side of the bridge to V_{PM} and the other side to $V_{PM} - 5$V, and powering the $V_{PM} - 5$V source after V_{PM}.

Compensating the gyroscope ZRO with stress and temperature is an ongoing work. The uncompensated Allan deviation graph in Figure 10 shows the performance of a second SOI-MEMS gyroscope with a bias instability of 6.1°/hr and angle random walk (ARW) of 46.6°/hr/√Hz. The gyroscope was operated at 50 Hz mismatch with closed-loop sense and quadrature cancellation in this test. The stress and temperature compensation is expected to remove a significant portion of the long term rate random walk.

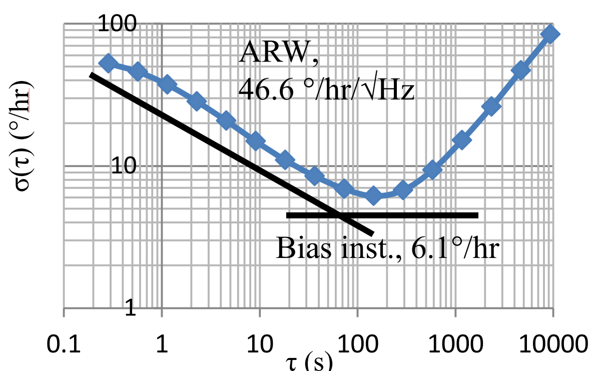

Figure 10: Uncompensated Allan deviation test results of a second gyroscope sample.

CONCLUSIONS

The importance of external stress on the MEMS gyroscope ZRO and SF has been shown using on-chip sensors that measure the stress and temperature separately and validated through a four-point bending test-bed. Drive and sense comb gap mismatches arising from stress-induced anchor displacements are believed to be the source of the ZRO shifts. The changes in the stress and ZRO were not captured by the temperature sensor indicating the importance of on-chip stress sensors on the die. This study shows the possible benefits of having on-chip stress sensors in addition to temperature sensors on the MEMS die for gyroscope bias compensation.

ACKNOWLEDGEMENTS

This work was supported by Defense Advanced Research Projects Agency (DARPA) under agreement number FA8650-08-1-7824. The work was also partially supported by the National Science Foundation Grant #CNS 0941497 as part of the Cyber-enabled Discovery and Innovation (CDI) program.

REFERENCES

[1] A. D. Challoner, H. H. Ge, and J. Y. Liu, "Boing disc resonator gyroscope", *Proc. PLANS 2014,* Monterey, May 5-8, 2014, pp. 504-514.

[2] S. A. Zotov, B. R. Simon, G. Sharma, A. A. Trusov, and A. M. Shkel, "Utilization of mechanical quadrature in silicon MEMS vibratory gyroscope to increase and expand the long term in-run bias stability", *Proc. ISISS 2014,* Laguna Beach, February 25-26, 2014, pp. 145-148.

[3] S. S. Walwadkar, and J. Cho, "Evaluation of die stress in MEMS packaging: Experimental and theoretical approaches", *IEEE Trans. on Components and Packaging Tech.*, vol. 29, no. 4, pp. 735-742, December 2006.

[4] E. Tatar, C. Guo, T. Mukherjee, and G. K. Fedder, "Interaction effects of temperature and stress on matched-mode gyroscope frequencies", *Proc. TRANSDUCERS 2013,* Barcelona, June 16-20, 2013, pp. 2527-2530.

[5] E. Tatar, T. Mukherjee, and G. K. Fedder, "Effects of stress on matched-mode gyroscope frequencies", *Proc. ISISS 2014,* Laguna Beach, February 25-26, 2014, pp. 1-4.

[6] E. Tatar, T. Mukherjee, and G. K. Fedder, "Simulation of stress effects on mode-matched MEMS gyroscope bias and scale factor", *Proc. PLANS 2014,* Monterey, May 5-8, 2014, pp. 16-20.

[7] V. Chidambaram, X. Ling, and C. Bangtao, "Titanium-based getter solution for wafer-level MEMS vacuum packaging", *J. Electronic Materials,* vol. 42, no.3, pp. 485-491, 2013.

CONTACT

E. Tatar, tel: +1-412-268-6606; etatar@andrew.cmu.edu